



Spontaneous chiral self-assembly of achiral AIEgens into AIEgen-silica hybrid nanotubes†

Cite this: *Chem. Commun.*, 2019, 55, 14438

Received 4th September 2019,
Accepted 4th November 2019

DOI: 10.1039/c9cc06873b

rsc.li/chemcomm

Wanning Zhang,^{‡a} Hui Chang,^{‡a} Jing Ai,^b Shunai Che,^{ib,ab} Yingying Duan^{ib,*b} and Lu Han^{id,*b}

Antipodal chiral AIEgen-silica hybrid mesostructures were fabricated by spontaneous chiral self-assembly of the achiral amphiphilic AIEgen 2-[4-(1,2,2-triphenylethenyl)phenoxy]-acetic acid via a co-structure directing route in the absence of any symmetry-breaking agent. The produced AIEgen-silica hybrid mesostructured nanotubes showed chiral features with optical activity originating from J-aggregation with an excess of one stereochemical hand of the helical conformation of the AIEgen.

Chiral symmetry breaking is a ubiquitous phenomenon throughout the universe from the elementary particle scale to the planetary scale.^{1,2} The enthusiasm and curiosity about the formation of chiral species have motivated researchers from interdisciplinary fields. Symmetry breaking of superstructures by chiral molecules has been widely studied,³ and chiral inorganic materials have been induced using chiral molecules as symmetry-breaking molecules.⁴ It has been realized that the spontaneous symmetry breaking of a superstructure without a chiral species requires achiral molecules with high rigidity and complexity, such as J-aggregates of 4-sulfonylphenylporphyrin derivatives.⁵

As a typical aggregation-induced emission (AIE) molecule, tetraphenylethene (TPE) and its derivatives exhibit a wide range of prospects in applications such as sensors, optoelectronic materials, and catalysts due to their high fluorescence quantum

yields and ready functionalization.^{6,7} Notably, chiral TPE derivatives constitute one of the promising candidates for applications in advanced chiral luminescent devices.⁸ The aggregation-induced chirality effect of superstructures based on TPE derivatives has been mostly achieved as a result of the elaborate design of the peripheries of the TPE scaffold,⁹ the decoration of the TPE core with chiral pendants^{10,11} and introduction of chiral molecules into the TPE frameworks.¹² Spontaneous chiral symmetry breaking of TPE and its derivatives with propeller-shaped structures has been reported in the crystalline or superstructure states.¹³ The chirality of the TPE-based superstructures can be controlled by adjusting the solvent composition and polarity.¹⁴ The chirality of these TPE-core compounds has been demonstrated using a combination of comprehensive solid-state chiroptical spectroscopy and theoretical calculations.¹⁵ However, the synthesis of mesostructured AIEgen-inorganic hybrid nanomaterials is still challenging, while the formation of an inorganic framework would lead to the increased stability and enhanced optical properties of AIE materials.

Various highly ordered mesostructured organo-silica hybrid and pure silica materials have been synthesized through co-operative self-assembly of amphiphilic molecules and a silica source, with the self-assembly relying on the formation of electrostatic and hydrogen bonding interactions.¹⁶ The co-structure directing route proposed by Che *et al.*¹⁷ can immobilize the self-assembled structures of anionic amphiphilic molecules with silica frameworks through proper interactions between amphiphilic molecules and inorganic species using cationic organosilanes as co-structure directing agents (CSDAs). In this work, 2-[4-(1,2,2-triphenylethenyl)phenoxy]-acetic acid (TPEA) was used as an anionic amphiphilic compound, quaternized aminosilane *N*-trimethoxysilylpropyl-*N,N,N*-trimethylammonium chloride (TMAPS) as a CSDA, and tetraethyl orthosilicate (TEOS) as a silica precursor to self-assemble into chiral AIEgen-silica hybrid mesostructures. TPEA has been shown to display a propeller-shaped set of four aryl blades that readily stack into a chiral superstructure. In an alkaline solution, the negatively charged carboxylate groups of TPEA have been shown to electrostatically interact with the positively charged quaternary ammonium groups of TMAPS, while the

^a School of Chemistry and Chemical Engineering, State Key Laboratory of Composite Materials, Shanghai Key Laboratory for Molecular Engineering of Chiral Drugs, Shanghai Jiao Tong University, 800 Dongchuan Road, Shanghai, 200240, P. R. China

^b School of Chemical Science and Engineering, Tongji University, 1239 Siping Road, Shanghai, 200092, P. R. China. E-mail: luhan@tongji.edu.cn, yyduan@tongji.edu.cn

† Electronic supplementary information (ESI) available: Experimental section, ¹H and ¹³C NMR spectra of TPE-1 and TPEA (Fig. S1 and S2), elemental analysis results of the TPEA (Table S1), SEM images of right-handed ribbon and R-CASN (Fig. S3 and S4), UV-Vis spectra of TPEA (aq.), TPEA and CASN (Fig. S5), *g* value of antipodal CASN (Fig. S6), AIE feature of TPEA (Fig. S7), photophysical data of TPEA and CASN (Table S2), photographs of TPEA and CASN under natural light and under 365 nm-wavelength UV light (Fig. S8), TGA thermograms of TPEA and CASN (Fig. S9), and *g*_{lum} value of the antipodal CASN (Fig. S10). See DOI: 10.1039/c9cc06873b

‡ These authors contributed equally to this work.

silane site of TMAPS can be co-condensed with TEOS to form the inorganic wall. Here, antipodal chiral lamellar mesostructured AIEgen-silica hybrid hollow nanotubes (CASNs) displaying optical activity were synthesized. The four phenyl rings of TPEA can spontaneously form clockwise or counterclockwise arrangements relative to the olefinic plane, resulting in a J-aggregated helical ribbon with an excess of one of the stereochemical conformations of TPEA. The left-handed CASN is denoted as L-CASN and the right-handed CASN as R-CASN, with the determination of handedness here based on the chiroptical response (*vide post*). The procedure used to synthesize TPEA and the results of the synthesis are illustrated in (Experimental section and Fig. S1 and S2, ESI[†]). And the results of the elemental analysis of TPEA are provided in Table S1 (ESI[†]).

Analysis of the X-ray diffraction patterns of the CASN indicated a typical lamellar organization (Fig. 1a). Two well-resolved reflections at $2\theta = 2.5^\circ$ and 5.0° were observed from both L- and R-CASN, and were indexed as first- and second-order reflections of the lamellar structure with a *d*-spacing of ~ 3.5 nm.

As shown in Fig. 1b, the L-CASN sample was mostly composed of uniform open-ended tubes with outer diameters of 200–400 nm. The lengths of the hollow nanotubes ranged widely, from hundreds of nanometers to dozens of micrometers. As shown in the magnified SEM image (Fig. 1c), very few imperfect nanotubes were observed, and they showed each an incomplete morphology of helical ribbons. The pitch length of the left-handed ribbon was determined to be ~ 350 nm, (the right-handed ribbon is shown in Fig. S3, ESI[†]). This phenomenon implied that the chiral hollow nanotubes was transformed from helical ribbons by merging edges. The R-CASN sample exhibited a hollow nanotube morphology (R-CASN is shown in Fig. S4, ESI[†]). The acquired TEM images (Fig. 1d and e) of the L-CASN sample displayed a hollow tube structure with inner diameters of 100–180 nm and wall thickness values of 50–110 nm. Lamellar architectures with *d*-spacings of ~ 3.5 nm were observed in the wall, consistent with the XRD pattern.

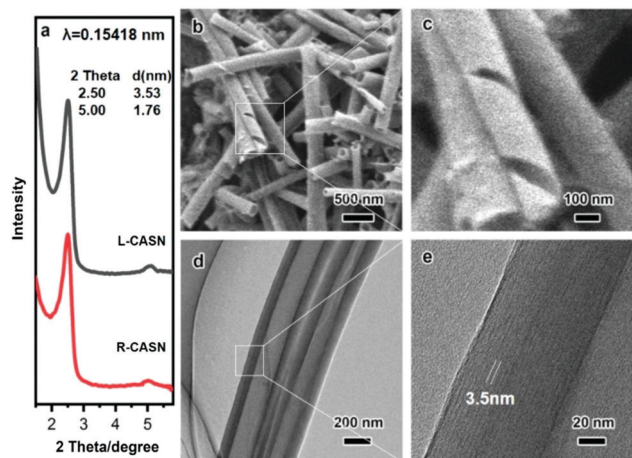


Fig. 1 XRD patterns (a) of as-made L- (black) and R-CASN (red), SEM images (b and c) and TEM images (d and e) of L-CASN. The synthetic molar composition of each CASN was TPEA:NaOH:TMAPS:TEOS:H₂O = 1:1:1.5:7:24 000.

The acquired diffuse reflection ultraviolet-visible (DRUV-Vis) spectra of the CASN sample are shown in Fig. S5 (ESI[†]). The CASN absorption band from 240 to 410 nm was attributed to the overlap of various characteristic TPEA absorption bands. The TPEA sample yielded dual bands, at 260 nm and 360 nm, while the solution of TPEA exhibited dual absorption bands, at 244 nm and 318 nm, owing to the π - π^* electronic transition in a single molecule, while the longer-wavelength band at 360 nm was ascribed to electronic transitions based on intermolecular interactions similar to those seen in the case of J-aggregates.¹⁸

Non-racemic molecular or mesoscopic chiral chromophores have been shown to display optical activity (OA). Therefore, the chiral stacking of achiral TPEA should endow the CASN with OA. The ground-state chirality of CASNs can be detected from a diffuse reflection circular dichroism (DRCD) analysis. As shown in Fig. 2a, mirror-image-related CD spectra curves were obtained for the antipodal CASN products, and corresponded to the DRUV-Vis spectra. The DRCD spectrum of L-CASN exhibited a negative signal from 200 to 326 nm, attributed to the π - π^* electronic transition in a single TPEA molecular unit. In contrast, the assembled structure exhibited a positive-negative bisignate signal ranging from 326 to 450 nm due to electronic transitions based on intermolecular interactions of the TPEA scaffolds.¹⁸ Notably, a medium with a left-handed helical structure absorbs right-handed circularly polarized light and exhibits CD signals changing from negative to positive with a shortened wavelength.¹⁹ Therefore, it can be inferred that the TPEA surfactant formed a left-handed helical arrangement in the L-CASN sample and a right-handed helical arrangement in the R-CASN sample. The Kuhn anisotropy factor *g* was also plotted, as shown in Fig. S6 (ESI[†]), for the as-synthesized CASN. Based on the results of 160 experiments (Fig. 2b), spontaneous symmetry breaking of the CASN was stochastic and unmanageable during the self-assembly process.

The AIE feature of TPEA is illustrated in Fig. S7 (ESI[†]). The fluorescence intensity emerged at a wavelength of ~ 386 nm for TPEA and showed a greater than 3-fold increase with the aggregation of TPEA through addition of ether into the TPEA ethanol solution. In a confocal laser scanning microscopy (CLSM) study, the pure TPEA showed an irregular shape and emitted weak blue light (Fig. 3a). After the formation of the CASNs, the cylindrical objects emitted stronger cyan light (Fig. 3b), occurring with an obvious red-shift, which was consistent with the emission spectra of the TPEA and CASN samples. Photographs of the TPEA and CASN samples

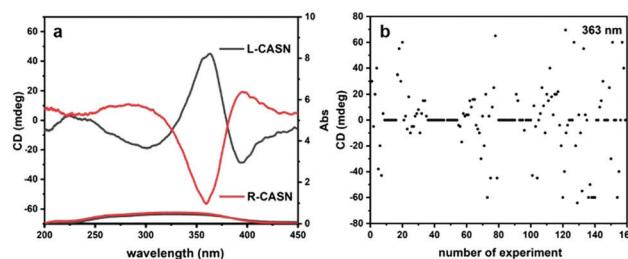


Fig. 2 DRCD spectra (a) of as-made L- (black) and R-CASN (red). CD values (b) at 363 nm for each of the 160 experiments.

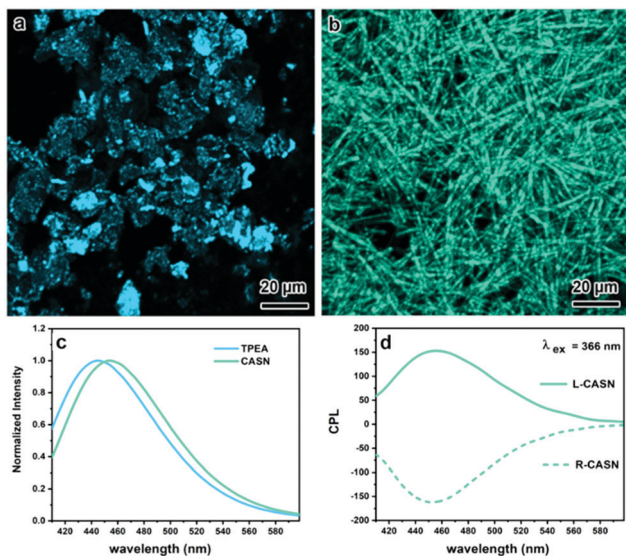
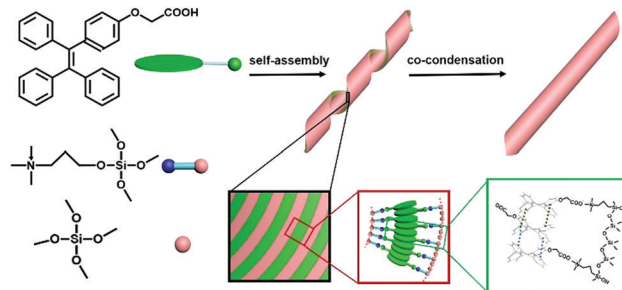


Fig. 3 CLSM images of pure TPEA surfactant (a) and L-CASN (b) and fluorescence spectra (c) of the pure TPEA surfactant (blue) and the CASN (cyan). CPL spectra (d) of antipodal samples. $\lambda_{\text{ex}} = 366 \text{ nm}$.

under natural light and 365 nm-wavelength UV light are shown in Fig. S8 (ESI[†]). The TPEA and CASN samples showed fluorescence lifetimes of 4.41 ns and 5.58 ns, and emission quantum yields of 0.41 and 0.57, respectively (Table S2, ESI[†]). These results indicated the ordered arrangement of TPEA in the silica wall can give rise to fluorescence aggregation-induced emission with relatively high efficiency, which can be ascribed to the intramolecular motions²⁰ of the four phenyl rings of TPE being restricted by the rigid inorganic silica wall. Besides, the CASN showed higher thermal stability than the pure TPEA (Fig. S9, ESI[†]), reflecting the silica wall of AIEgen-silica hybrid materials showing a certain ability to protect the TPEA.

Fig. 3c depicts the emission behaviors of the TPEA and CASN samples in aggregated states. The TPEA sample emitted light at a wavelength of 443 nm. Compared to this emission, that of the CASN sample was red-shifted, to 453 nm, indicating that the close stacking of the TPEA molecules increased π - π conjugation.²¹ When the molecules formed a lamellar micelle, the TPE core may have become more coplanar and the surfactant may have possessed better electronic conjugation and experienced stronger intermolecular interactions, causing the red-shifted emission of the CASN sample.

Furthermore, OA of the CASN sample in the electronic excited state involved in the emission process was indicated according to the results of a circularly polarized luminescence (CPL) study. Left-handed helical structured materials prefer to emit left-handed circularly polarized light and display positive CPL signals.²² CPL intensities of antipodal CASNs as strong as 150 mdeg and a g_{lum} value as large as 0.02 with an excitation wavelength λ_{ex} of 366 nm were measured (Fig. S10, ESI[†]). The positive CPL signal from the L-CASN sample at this excitation wavelength confirmed the left-handed helical arrangement of the TPEA surfactant. The slight differences between the CPL signals of different CASNs may be attributed to the variation of the helicity of TPEA.



Scheme 1 Schematic drawing of the formation of L-CASN.

From the above data, a mechanism was derived to explain the determination and amplification of chirality from the molecular level to the mesoscopic level according to majority-rules principle (Scheme 1).²³ In the solution state, the four phenyls of TPEA are free to rotate and the TPEA is achiral. However, in the co-structure directing route, the stereochemical conformation is immobilized as a result of silica condensation, which consequently leads to either an anticlockwise (M) or clockwise (P) arrangement. In the early stages, once the formation of the P-conformer TPEA predominates over that of the M-conformer, the achiral TPEA of the solution could transform into P-conformer TPEA as a result of π - π stacking and the steric repulsion of the adjacent phenyl units and the reverse process forming achiral TPEA could also occur. The transformation in the preferential configuration further propagates into the formation of helical ribbon J-aggregate. With the silica polymerization, the multi-lamellar CASN hybrids are finally formed. On the other hand, if P-conformer and M-conformer TPEA were formed in equal amounts, racemic CASN would be fabricated with the absence of CD signals. The symmetry-breaking process is stochastic and unmanageable.

In summary, we fabricated chiral CASN hybrid hollow nanotubes from precursors without any symmetry-breaking agent. The CD and CPL signals of the samples demonstrated the chirality and circularly polarized AIE properties of antipodal CASNs. Our results may provide a new, convenient and efficient method for immobilizing a particular stereoisomer of a molecular structure, especially with a focus on propeller-shaped structures with a central stator and surrounding rotor. This research may also help explain the origin of chirality and extend the applications of AIE molecules to those involving the formation of inorganic-organic nanomaterials.

This work was supported by the National Natural Science Foundation of China (21873072, 21571128, 21601123) and Shanghai Rising-Star Program (17QA1401700). The authors thank the Instrumental Analysis Centre of Shanghai Jiao Tong University for CD measurements.

Conflicts of interest

There are no conflicts to declare.

Notes and references

- H. Qiu and S. Che, *Chem. Soc. Rev.*, 2011, **40**, 1259–1268.
- K. Soai, *Proc. Jpn. Acad., Ser. B*, 2019, **95**, 89–110.

- 3 J. C. Mitchell, J. R. Harris, J. Malo, J. Bath and A. J. Turberfield, *J. Am. Chem. Soc.*, 2004, **126**, 16342–16343.
- 4 S. Liu, L. Han, Y. Duan, S. Asahina, O. Terasaki, Y. Cao, B. Liu, L. Ma, J. Zhang and S. Che, *Nat. Commun.*, 2012, **3**, 1215–1221.
- 5 J. M. Ribo, J. Crusats, F. Sague, J. Claret and R. Rubires, *Science*, 2001, **292**, 2063–2066.
- 6 B. Xu, J. He, Y. Mu, Q. Zhu, S. Wu, Y. Wang, Y. Zhang, C. Jin, C. Lo, Z. Chi, A. Lien, S. Liu and J. Xu, *Chem. Sci.*, 2015, **6**, 3236–3241.
- 7 H. Feng, Y. Yuan, J. Xiong, Y. Zheng and B. Z. Tang, *Chem. Soc. Rev.*, 2018, **47**, 7452–7476.
- 8 L. Chen, Y. Jiang, H. Nie, R. Hu, H. S. Kwok, F. Huang, A. Qin, Z. Zhao and B. Z. Tang, *ACS Appl. Mater. Interfaces*, 2014, **6**, 17215–17225.
- 9 C. Liu, G. Yang, Y. Si and X. Pan, *J. Phys. Chem. C*, 2018, **122**, 5032–5039.
- 10 J. Xiong, W. Xie, J. Sun, J. Wang, Z. Zhu, H. Feng, D. Guo, H. Zhang and Y. S. Zheng, *J. Org. Chem.*, 2016, **81**, 3720–3726.
- 11 M. Kawai, A. Hoshi, R. Nishiyabu and Y. Kubo, *Chem. Commun.*, 2017, **53**, 10144–10147.
- 12 J. Xiong, H. Feng, J. Sun, W. Z. Xie, D. Yang, M. Liu and Y. S. Zheng, *J. Am. Chem. Soc.*, 2016, **138**, 11469–11472.
- 13 T. Kawasaki, M. Nakaoda, N. Kaito, T. Sasagawa and K. Soai, *Origins Life Evol. Biospheres*, 2010, **40**, 65–78.
- 14 D. D. La, A. Anuradha, A. Gupta, M. Al Kobaisi, A. Rananaware and S. V. Bhosale, *Sci. Rep.*, 2015, **5**, 15652–15663.
- 15 D. Li, R. Hu, D. Guo, Q. Zang, J. Li, Y. Wang, Y. Zheng, B. Z. Tang and H. Zhang, *J. Phys. Chem. C*, 2017, **121**, 20947–20954.
- 16 H. Chang, W. Mao, Y. Duan, W. Zhang, C. Zhou, L. Han, L. Li and S. Che, *J. Mater. Chem. C*, 2019, **7**, 346–353.
- 17 S. Che, Z. Liu, T. Ohsuna, K. Sakamoto, O. Terasaki and T. Tatsumi, *Nature*, 2004, **429**, 281–284.
- 18 Y. J. Jin, H. Kim, J. J. Kim, N. H. Heo, J. W. Shin, M. Teraguchi, T. Kaneko, T. Aoki and G. Kwak, *Cryst. Growth Des.*, 2016, **165**, 2804–2809.
- 19 Y. Duan, L. Han, J. Zhang, S. Asahina, Z. Huang, L. Shi, B. Wang, Y. Cao, Y. Yao, L. Ma, C. Wang, R. K. Dukor, L. Sun, C. Jiang, Z. Tang, L. A. Nafie and S. Che, *Angew. Chem., Int. Ed.*, 2015, **54**, 15170–15175.
- 20 B. Gui, N. Yu, Y. Meng, F. Hu and C. Wang, *J. Polym. Sci., Part A: Polym. Chem.*, 2017, **55**, 1809–1817.
- 21 A. Rananaware, D. D. La and S. V. Bhosale, *RSC Adv.*, 2015, **5**, 56270–56273.
- 22 J. Kumar, T. Nakashima and T. Kawai, *J. Phys. Chem. Lett.*, 2015, **6**, 3445–3452.
- 23 M. M. J. Smulders, P. J. M. Stals, T. Mes, T. F. E. Paffen, A. P. H. J. Schenning, A. R. A. Palmans and E. W. Meijer, *J. Am. Chem. Soc.*, 2010, **132**, 620–626.